CERN - EUROPEAN ORGANIZATION FOR NUCLEAR RESEARCH

Submitted to
Nuclear Physics B

CERN/EP/PHYS 78-13
21 June 1978

# DENSITY, CHARGE AND TRANSVERSE MOMENTUM CORRELATIONS OF PARTICLES IN NON-DIFFRACTIVE PROTON-PROTON COLLISIONS AT $\sqrt{s}$ = 52.5 GeV

CERN-Collège de France-Heidelberg-Karlsruhe Collaboration

D. DRIJARD, H.G. FISCHER, R. GOKIELI(*), P.G. INNOCENTI, V. KORBEL(**), A. MINTEN, A. NORTON, R. SOSNOWSKI(*), S. STEIN(***), O. ULLALAND and H.D. WAHL
CERN, European Organization for Nuclear Research, Geneva, Switzerland

P. BURLAUD, M. DELLA NEGRA(+), G. FONTAINE, P. FRENKIEL, C. GHESQUIERE, D. LINGLIN(+) and G. SAJOT
Collège de France, Paris, France

H. FREHSE(++), E.E. KLUGE, A. PUTZER and J. STIEWE
Institut für Hochenergiephysik der Universität, Heidelberg, Germany

P. HANKE(++), W. HOFMANN(+++), W. ISENBECK, J. SPENGLER(+++) and D. WEGENER(+++)
Institut für Experimentelle Kernphysik der Universität (TH) Karlsruhe, Germany

(*) Now at Institute for Nuclear Research, Warsaw, Poland

(**) Now at DESY, Hamburg, Germany

(***) Now at SLAC, Stanford, USA

(+) Now at LAPP, Annecy, France

(++) Now at CERN, Geneva, Switzerland

(+++) Now at Institut für Physik der Universität Dortmund, Germany

HW/mk

ABSTRACT

Inelastic events with an observed charged multiplicity $n_{obs} \geq 7$ have been studied at the CERN Intersecting Storage Rings using the Split Field Magnet detector. Correlations of particle densities, charges and transverse momenta have been determined and a phenomenological analysis in the framework of cluster models has been performed. A good description of all results is obtained if one allows for charged clusters, produced in a mechanism with limited charge exchange. The mean transverse momentum of clusters is (0.65 ± 0.10) GeV/c. Short range correlations of particles of like charge due to the Bose-Einstein effect can be described as a second order interference phenomenon with a radius R = (1.34 ± 0.31) fm and a lifetime of $c\tau$ = (1.38 ± 0.60) fm for the pion source.

## 1. INTRODUCTION

The prominent feature of non-diffractive multiparticle events at high energies is the presence of short range correlations in rapidity, which have been explained in the framework of cluster models [1,2]. The observed short range correlations depend on the charge and the transverse momenta of the secondaries [3].

It has been pointed out [3,4] that a stringent check of the models for multiparticle production and in particular of the different versions of the cluster model is only possible in an analysis which describes all experimentally accessible correlation data with a single parameter set. Since phase-space effects dominate the measured correlations at medium energies, it is important to take data at the highest energies in order to isolate the dynamical features of multiparticle production processes. It is the aim of the present paper to meet these two conditions.

Data were taken at a centre of mass energy of $\sqrt{s}$ = 52.5 GeV with the Split Field Magnet spectrometer. In order to minimize contributions from diffractive reactions, only events with a reconstructed charged multiplicity $n_{obs} \geq 7^{(*)}$ were taken into account in the present analysis. The measured correlations of the particle densities, charge densities and transverse momenta of the produced particles are compared to the predictions of cluster models.

The outline of the paper is as follows: in sect. 2 we give a short description of the detector and the acceptance corrections applied to the raw data. Sect. 3 contains the definitions of the experimental distributions studied, as well as a summary of the basic assumptions of the different cluster model versions and their physical meaning. The experimental data and their comparison with the predictions of the cluster models are presented in sect. 4, and sect. 5 gives a summary of the results and our

---

(*) This value corresponds to the average number of reconstructed tracks in inelastic events.

conclusions. Appendix A contains additional information about the definition of and the relations between the distributions studied in this paper. The technical details of the model calculations are summarized in Appendix B.

A more detailed account of the experimental procedures and the data analysis can be found in ref. [5].

## 2. DETECTOR AND EXPERIMENTAL PROCEDURE

### 2.1 Detector

The experiment was performed at the CERN Intersecting Storage Rings (ISR) with the Split Field Magnet (SFM) detector, which allows to measure the momenta of charged particles in nearly the full solid angle. The detector consists of a magnet with a maximum field strength of 1 Tesla surrounding the interaction region I4 of the ISR. The magnetic volume is filled with Multiwire Proportional Chambers (MWPC) divided into three telescopes: two forward telescopes [6], each consisting of 14 MWPC and a vertex detector, described in [7]. Information about the performance of the detector can be found in previous publications [8].

### 2.2 Trigger

The MWPC's were used in a self-triggering mode [9]. Wires of the MWPC were associated in groups of 256 to deliver fast signals. These signals were combined to define the time of the event by an OR of all wires of the detector. A geometrical pattern for the "minimum bias" trigger was defined by a fast majority coincidence of at least three chambers in any of the three telescopes. This trigger essentially required the presence of at least one reconstructable track. After the exclusion of elastic events, the cross section seen by this trigger amounts to $\simeq$ 95% of the inelastic cross section. The total number of triggers taken was $\sim 4.5 \cdot 10^5$.

## 2.3 Data processing and corrections

The raw data were processed with the SFM off-line program chain [10]. Approximately 90% of the "good" triggers (i.e. those not rejected for purely technical reasons) gave at least one reconstructed track, yielding $\sim$ 370 000 useful events. The present analysis is based on $\sim$ 60% of the total data sample ($\sim$ 120 000 events with more than seven reconstructed tracks).

After track reconstruction, the data were corrected for geometrical acceptance losses in the detector, losses due to decay and secondary interactions and inefficiencies of the analysis chain. In previous analyses [8], Monte-Carlo tracks were used to establish acceptance tables by an integration technique. In the present analysis, the acceptance corrections were determined from a subset of the data, using the fact that the particle density $\rho$ of the produced particles in the proton-proton centre of mass system is independent of the azimuthal angle $\phi$ and symmetric in the rapidity y, i.e. $\rho(y,\phi) = \rho(|y|)$. From previous studies [8] it is known that for every region in y and transverse momentum $p_T > 0.1$ GeV/c, an interval in $\phi$ can be found in which the full acceptance of the detector ($\sim$ 95%) is reached and in which inefficiencies of the program chain are small (i.e. at the level of a few percent). Thus a suitable binning in y, $p_T$ and $\phi$ was chosen for tabulation of the acceptance weights. Only tracks with a momentum error $\Delta p/p < 40\%$ were considered and the correction for losses due to this selection is included in the weight factor. The average correction factor applied to the data is $\sim$ 1.5. The distributions obtained by correcting with this method agree in the overlapping phase-space regions with those obtained by different techniques [8].

Since the acceptance of the detector is poor for particles with low transverse momenta, the experimental distributions were determined for $p_T > 0.1$ GeV/c (in some cases > 0.175 GeV/c) and extrapolated to $p_T = 0$ (when necessary). After corrections (and extrapolation to $p_T = 0$), the average charged multiplicity at $\sqrt{s} = 52.5$ GeV found in this experiment

is $\langle n_{ch} \rangle = 10.8 \pm 1.1$, to be compared with the recently published value of $11.8 \pm 0.1$ [11]. The total charge of the detected secondaries is $Q_{det} = 1.95 \pm 0.10$, in good agreement with the expected value of 2.

For all calculations, the pion mass was assigned to the particles, except for positive particles with $|x| > 0.5$, which were assumed to be protons (x = reduced longitudinal momentum in the c.m. system).

## 3. PHENOMENOLOGICAL ANALYSIS

### 3.1 General definitions

A major aim of this analysis is the study of correlations between two hadrons in the reaction

$$pp \rightarrow h_1 + h_2 + X, \qquad (1)$$

as far as number, charge and transverse momentum of particles are concerned. The particles $h_1$, $h_2$ are characterized by their charge $Q_i$ and their kinematic variables $\vec{p}_i = \{y_i, p_{Ti}, \phi_i\}$ $(i = 1, 2)$ (see table 1 for definitions). Most of the experimental distributions are presented as functions of rapidity y, in which case integration over the other variables is implicit. In addition to the standard single-particle and two-particle densities and correlation functions (table 1), we use "associated" (conditional) densities [12] of particle number, charge and transverse momentum. These associated quantities are obtained by selecting events with a particle $h_2$ (the "selected" or "software trigger" particle) in a phase-space interval around $\vec{p}_2$, and then evaluating the quantity in question (particle density, charge density, etc.) for the particles $h_1$ (at $\vec{p}_1$) of the rest of the event (excluding the selected particle).

(a) Particle and charge densities:

The associated particle density $\rho^{Q_1Q_2}(y_1|y_2)$ is the density of particles of charge $Q_1$ at rapidity $y_1$, under the condition that there is a particle of charge $Q_2$ at rapidity $y_2$. It is related to the inclusive two-particle density by, e.g.

$$\rho^{+-}(y_1|y_2) = \rho^{+-}(y_1, y_2)/\rho^{-}(y_2).$$

The associated charge density $q(y_1|Q_2,y_2)$ is the net charge density at rapidity $y_1$ under the condition that there is a particle of charge $Q_2$ at rapidity $y_2$. Instead of using this quantity, we prefer to study the associated charge density balance $\Delta q(y_1|y_2)$, defined by

$$\Delta q(y_1|y_2) = q(y_1|-,y_2) - q(y_1|+,y_2) \ , \qquad (2)$$

i.e. it is the change in the associated charge density at $y_1$ when the selected particle $h_2$ of negative charge is replaced by one with positive charge. From the definition it is clear that

$$\int \Delta q(y_1|y_2)\, dy_1 = 2,$$

independent of $y_2$ and the charge of the initial particles (Appendix A). The quantity (2) can be expressed in terms of two-particle correlation functions and is related to the charge transfer correlation function [13] (Appendix A).

One advantage of choosing $\Delta q$ is that the influence of acceptance corrections for this quantity is smaller than for the charge density itself [5]. Moreover, it allows a clearer separation between contributions to charge compensation arising from central production and fragmentation, which seem to have a different dynamical origin [14].

(b) Transverse momentum compensation:

For the purpose of investigating the locality of transverse momentum conservation, we study the associated compensating transverse momentum density $\Pi_T(y|y')$, defined by

$$\Pi_T(y|y')dy = - \langle \sum_i \vec{p}_{Ti} \cdot (\vec{p}'_T/|\vec{p}'_T|) \rangle, \qquad (3)$$

where $\vec{p}'_T$ and y' specify the selected particle. The sum is taken over all (charged) particles with rapidities $y_i$ in an interval around y, and the average is taken over the sample of events which have a particle at rapidity y'. Thus, $\Pi_T(y|y')$ is the total net component of transverse momentum (per unit of rapidity) at rapidity y opposite to the direction of the transverse momentum of the selected particle at y'.

From momentum conservation follows that

$$\int \Pi_T(y|y')dy = \varepsilon \langle p_T(y') \rangle,$$

where $\langle p_T(y') \rangle$ is the average transverse momentum of particles at rapidity y'; $\varepsilon = 1$ if the sum in (3) is extended over all particles (neutrals included); if only charged particles are included, $\varepsilon$ is expected to be $\sim 2/3$.

This problem of unseen neutrals (and remaining acceptance losses) is avoided by using a different quantity, the associated average compensating transverse momentum $\pi_T(y_1|y_2)$, defined by

$$\pi_T(y_1|y_2) = \Pi_T(y_1|y_2)/\rho(y_1|y_2). \qquad (4)$$

This quantity is independent of the density of particles and therefore also better suited to study global effects in the central region (sect. 4.4).

## 3.2 Cluster models

### 3.2.1 General features

In cluster models, non-diffractive multiparticle production is assumed to proceed via two independent steps, namely the production of clusters and their subsequent decay into the particles observed in the final state. In all model versions considered in this paper, production of both leading and central clusters is taken into account, in much the same way as in the analysis of ref. [4]. The central clusters are assumed to be uniformly distributed in rapidity with a density $\rho_c$, over a rapidity range which depends on the missing mass with respect to the two leading clusters (Appendix B and ref. [4]).

The model calculations have been performed using the Monte-Carlo method. Details about model and Monte-Carlo program are given in Appendix B, and the determination of the free parameters is described in sects 4.1 and 4.4.

### 3.2.2 Transverse momentum dependence

As far as the transverse momentum dependence of cluster production is concerned, we consider three different models [3]

- the uncorrelated jet model (UJM) [15];
- the uncorrelated link model (ULM) [16];
- the correlated link model (CLM) [17].

In the UJM, the transition matrix element $T_n$ for the production of n clusters is given by a factorized form in the transverse momenta $\vec{k}_{Ti}$ of the clusters (fig. 1)

$$|T_n|^2 \sim \prod_{i=1}^{n} f(k_{Ti}^2).$$

The only correlation between cluster transverse momenta is then due to transverse momentum conservation.

In the ULM, the matrix element factorizes in functions of the transverse momenta $\vec{q}_{Ti}$ exchanged between two clusters adjacent in rapidity (i.e. the transverse momentum transfer at each link)

$$|T_n|^2 \sim \prod_{i=1}^{n-1} g(q_{Ti}^2),$$

while in the CLM, the matrix element factorizes in functions of the transverse momentum transfers at two neighbouring links

$$|T_n|^2 \sim g(q_{T1}^2) \prod_{i=1}^{n-2} G(\vec{q}_{Ti}, \vec{q}_{Ti+1}) \; g(q_{Tn-1}^2).$$

Both UJM and ULM can be considered as special cases of the CLM [17]. The functions f, g, G are fast decreasing functions of their arguments (in our calculation, gaussian dependences on $k_T$ and $q_T$ have been used).

In the UJM, the transverse momenta of the clusters are compensated globally. In the ULM, the transverse momentum correlation length $\lambda_T$ for clusters, i.e. the distance in rapidity over which the cluster transverse momenta are compensated, is of the order of 1 unit of rapidity. In the CLM, the correlation length is $\lambda_T \sim 3$.

3.2.3 Charge dependence

For the charge dependence of cluster production, three different assumptions have been considered:

- Independent emission of neutral clusters (IENC) [18].
- Independent emission of charged clusters (IECC) [4], where the charge of a cluster is only constrained by the overall charge conservation. In this analysis we specialize to the case that the produced clusters occur only in the three charge states ±1, 0. The charge correlation length $\lambda_Q$ for the compensation of the charge of a cluster by that of another cluster is expected to be $\lambda_Q \approx 3$ at the present energy $\sqrt{s}$ = 52.5 GeV.

- Emission of charged clusters with limited charge exchange (LCEX) [17,19] between clusters neighboured in rapidity. In our analysis we limit this exchange of charges to ±1, 0. The correlation length for this type of model is expected to be of the order $\lambda_Q \approx 1.5$.

It should be noted that the correlation lengths $\lambda_T$ and $\lambda_Q$ given above refer to the compensation of transverse momentum and charge of clusters and not of particles. The corresponding lengths observed for particles are expected to be increased due to the spread $\delta$ in rapidity of particles originating from the decay of one cluster, which is of the order $\delta \sim 0.7$ (sect. 4).

## 4. EXPERIMENTAL RESULTS AND COMPARISON WITH CLUSTER MODEL

### 4.1 One and two-particle densities

As mentioned earlier, for all distributions given in this paper, only events with a seen multiplicity of charged particles $n_{obs} \geq 7$ are used. The single particle and charge densities are shown in fig. 2. Fig. 3 shows the conditional two-particle correlation $C'(y_1|y_2)$ as a function of $y_1$ for three different values of $y_2$. As suggested by the cluster model [2], this correlation function can be parametrized by

$$C'(y_1|y_2 = 0) = (F/2\delta\sqrt{\pi}) \exp(-y_1^2/4\delta^2) + \alpha\rho(y_1),$$

where the first term corresponds to the short range contribution to the correlation (two particles from the same cluster) and the second term represents the long range part. The parameter F, the "strength" of the short range correlation, is related to moments of the charged multiplicity distribution of cluster decay

$$F = \frac{\langle K(K-1)\rangle}{\langle K\rangle},$$

where $K$ is the number of charged particles from the decay of one cluster.

The width $\delta \cdot \sqrt{2}$ of the short range correlation is related to the spread in rapidity of particles originating from the decay of the same cluster (table 2).

From a fit to $C'(y_1|0)$ of fig. 3 we obtain the following values for these two parameters:

$$F = 1.24^{+0.20}_{-0.13} \quad \text{and} \quad \delta = 0.67 \pm 0.05 \tag{5}$$

in good agreement with the results of previous analyses [20,21].

From the measured value of F, an estimate of the mean charged multiplicity $\langle\kappa\rangle$ of the cluster decay can be derived. For a $\delta$-distribution, one gets $\langle\kappa\rangle = 2.24$, while for a Poisson-distribution, a value $\langle\kappa\rangle = 1.24$ is obtained. The best estimate is found to be [5]

$$\langle\kappa\rangle \sim 1.8 \tag{6}$$

(Appendix B). Since the density $\rho_C$ of central clusters and the single particle density $\rho(y = 0)$ are related by

$$\langle\kappa\rangle \cdot \rho_C = \rho(y = 0), \tag{7}$$

one can estimate the density of central clusters to be

$$\rho_C \simeq 1. \tag{8}$$

In order not to be biased by the selection of events with $n_{obs} \geq 7$, the full inclusive density $\rho$ was used in (7). The values of the parameters obtained are in good agreement with those found in [4].

The parameters describing the leading clusters can be determined from the charge density shown in fig. 2. A good fit to the charge density is obtained with an average charge of the leading cluster of $\langle Q_L \rangle \gtrsim 0.65$ and an average mass of $\langle M_L \rangle \sim 1.5$ GeV.

Thus, apart from the cluster transverse momentum, all free parameters of the cluster model are determined from three experimental distributions, namely the inclusive single particle density $\rho(y)$, the inclusive charge density $q(y)$ and the two-particle correlation function $C'(y_1|0)$. A summary of the free parameters, their determination and the values obtained are given in table 3.

The curves shown in figs 2 and 3 are the results of the calculation with the IECC model, using the values of the parameters given above. It should be noted that an equally good description of these distributions is also possible with the IENC and LCEX versions of the model (and the same parameters), i.e. more detailed experimental information is needed to discriminate between these models.

## 4.2 Charge correlations

To investigate the question of locality of charge conservation and, related to this, the charge dependence of cluster production, we study the associated charge density balance $\Delta q(y_1|y_2)$ as defined by eq. (2) (sect. 3.1). This quantity is shown in fig. 4 as a function of $y_1$, for four different values of rapidity $y_2$ of the selected particle. For comparison, also the associated particle density $\rho(y_1|y_2)$ is shown in the figure. The fact that $\Delta q(y_1|y_2)$ has a maximum at $y_1 \sim y_2$ for all four values of $y_2$, is a clear indication of local charge conservation. To show this more clearly, the charge density balance associated with a central particle ($|y_2| \leq 1$) is presented in fig. 5 as a function of the rapidity difference $\Delta y = |y_1 - y_2|$. The width (FWHM) of this distribution is $\sim 2.8$ units in rapidity and thus significantly larger than the value of $\sim 2$ expected from the IENC model(*). Indeed, the IENC model calculation

---

(*) Since clusters are neutral in the IENC model, the charge of a particle has to be compensated by other particles from the same cluster; therefore, $\Delta q$ should have approximately the same width as the two-particle correlation (fig. 3).

shown in fig. 5 is in strong disagreement with the data, while both versions of the charged cluster model give a good description of the experimental results.

Since the IECC and LCEX models should differ for large rapidity differences $\Delta y = |y_1 - y_2|$, we show in fig. 6 the model predictions for $\Delta q(y_1|y_2)$ associated with a particle at the edge of the central region, $y_2 = -2$. This is sufficiently far from the kinematical boundary that the influence of the charge transfer from leading particles should still be small in the region $y_1 > -2$. Comparison of the predictions with the data shows that the best description is obtained with the limited charge exchange model (LCEX), while the IECC model predicts too high a long range component of the charge compensation. From a study of charge transfers across rapidity gaps, as proposed in [19], one arrives at the same conclusions [5]. However, even though the LCEX model is favoured by the data, the IECC model cannot be ruled out definitely.

Fig. 7 shows the charge density balance $\Delta q(y_1,\phi_1|y_2,\phi_2)$ associated with a central particle ($|y_2| < 1.5$), for two different intervals of the transverse momentum $p_{T2}$ of the selected particle. For small transverse momenta $p_{T2}$ (fig. 7(a)), the charge is compensated mainly by particles opposite in $\phi$ with respect to the selected particle (strong concentration for $\Delta y \sim 0$, $\Delta\phi \sim 180^{\circ}$). For larger transverse momentum of the selected particle $h_2$, $p_{T2} > 0.5$ GeV/c (fig. 7(b)), a relative increase of $\Delta q$ near $\Delta\phi = 0$ is seen. These observations are in qualitative agreement with a behaviour expected for clusters with non-negligible transverse momentum (sect. 4.4). The strong depletion observed in fig. 7(a) for $\Delta y$, $\Delta\phi \sim 0$ is due to the Bose-Einstein effect.

## 4.3 Bose Einstein effect and second order interference

In figs 8(a), 8(b) the normalized correlation function $R'(\vec{p}_1,\vec{p}_2)$ (as defined in table 1) is plotted as function of $\Delta y = |y_1-y_2|$ and $\Delta\phi = |\phi_1-\phi_2|$ for particle pairs of like and unlike charge. For small $\Delta y$ and $\Delta\phi$ significant differences between the two correlation functions are observed. For equal charge pairs the correlation function shows a

maximum when the two particles are close in phase space, which is interpreted as a Bose-Einstein condensation of the two-pion system.

For a quantitative study of this effect it is convenient to use the variables $q_T$ and $q_L$ defined by (fig. 9)

$$\vec{q}_L = \hat{s} \cdot \left[ (\vec{p}_1 - \vec{p}_2) \cdot \hat{s} \right], \quad q_L = |\vec{q}_L|$$

$$\vec{q}_T = (\vec{p}_1 - \vec{p}_2) - \vec{q}_L, \qquad q_T = |\vec{q}_T|,$$

where $\hat{s}$ is a unit vector in the direction of the sum of the two particle momenta, $\hat{s} = (\vec{p}_1 + \vec{p}_2)/|\vec{p}_1 + \vec{p}_2|$. The "longitudinal" component $q_L$ serves as an approximation to the energy difference whose use is suggested by Kopylov and Podgoretskii [22]. The correlation function R' is shown in fig. 10 as a function of these two variables. For like charge pairs, a strong peak is observed for small values of $q_L$, $q_T$, while R' for unlike charge pairs is found to be independent of $q_L$, $q_T$ and $\sim 0$.

It has been proposed [22,23] to interpret this type of correlation as a second order interference phenomenon. According to this picture, the correlation function R' can be parametrized by

$$R'(q_L, q_T) = \beta \left\{ 1 + a \frac{4J_1^2 (q_T \cdot R)^2}{(q_T \cdot R)^2} \frac{1}{1 + (q_L \cdot \tau)^2} \right\}, \qquad (9)$$

where $\beta$ is a normalization constant, $J_1$ is the Bessel function of first order and R, $\tau$ measure the radius and lifetime of the pion source. The parameter a takes into account that not all detected particles are pions and also that there may be dynamic correlations which hinder the Bose-Einstein interference (ref. [24] for a more detailed discussion).

The distributions of fig. 10 have been fitted to the expressions

$$R'(q_T) = A_1 + A_2 \frac{4J_1^2 (q_T \cdot R)}{(q_T \cdot R)^2} \quad \text{for } q_L < 0.1 \text{ GeV/c}$$

and (10)

$$R'(q_L) = B_1 + B_2 \frac{1}{1 + (q_L \cdot \tau)^2} \quad \text{for } q_T < 0.2 \text{ GeV/c}.$$

The values of the parameters R and $\tau$ obtained by the fit are

$$R = (1.34 \pm 0.31) \text{ fm}$$

$$c\tau = (1.38 \pm 0.60) \text{ fm},$$

in agreement with the results of experiments performed at lower energies [24]. The interfering fraction of all pairs of like-charged particles (parameter a of eq. (9)) is found to be $\sim 0.4$.

## 4.4 Transverse momentum correlations

For the study of the locality of transverse momentum conservation, we use the two quantities $\Pi_T(y_1|y_2)$ and $\pi_T(y_1|y_2)$, defined in sect. 3.1 (eqs (3) and (4)). Fig. 11 shows the associated compensating transverse momentum density $\Pi_T(y_1|y_2)$ as a function of $y_1$, for four different values of rapidity $y_2$ of the selected particle. For a selected particle in the central region ($y_2 = 0, -1, -2$; figs 11(a), 11(b), 11(c)), $\Pi_T(y_1|y_2)$ is rather wide in $y_1$ and does not change very much with $y_2$. This shows that most of the transverse momentum is compensated globally. When the selected particle $h_2$ is nearer to the kinematical boundary, the distribution is somewhat narrower, which indicates a local compensation mechanism. The minimum at $y_1 \sim 0$ observed in fig. 11(a) is due to the Bose-Einstein effect described in the previous section.

The globality of transverse momentum conservation can be more clearly seen in the rapidity dependence of the average compensating transverse momentum $\pi_T(y_1|y_2)$ associated with a central particle ($|y_2| < 1$), shown in fig. 12. For large values of $\Delta y = |y_1 - y_2|$, $\pi_T(y_1|y_2)$ is nearly independent of $\Delta y$. As expected, it increases with the transverse momentum $p_{T2}$ of the selected particle $h_2$. The effects observed at small values of $\Delta y$ can be explained by a superposition of the Bose-Einstein effect and the influence of the transverse momentum of the central cluster.

A quantitative comparison of the predictions of the cluster model and the experimental results shows good agreement for the UJM model and the CLM model, if one assumes that clusters are produced with a mean transverse momentum of

$$\langle k_T \rangle = (0.65 \pm 0.10) \text{ GeV/c}. \qquad (11)$$

Using this result and the values of the other parameters obtained for the central clusters (sect. 4.1), one can derive [25] the average mass of central clusters as

$$\langle M_C \rangle \sim 1.3 \text{ GeV}. \qquad (12)$$

Similar conclusions have been obtained in a recent analysis of the transverse momentum behaviour of clusters [26], using published data on longitudinal and transverse correlations.

It should be noted that the value of $\langle k_T \rangle$ obtained in this analysis is comparable with the experimental value of the average transverse momentum of meson resonances of similar mass as the cluster mass (12) [27]. Hayot et al. [25] have derived a relation between the imaginary part of the elastic scattering amplitude and the multiparticle production amplitude. They have shown that for a UJM model this relation can only be fulfilled if the transverse momenta of the produced clusters are small, $\langle k_T^2 \rangle \approx 0.1 \text{ GeV}^2/c^2$. Such a small value can be excluded by the present analysis. In the framework of the CLM model, Le Bellac [1] has derived a relation between the cluster transverse momenta and the slope of the Pomeron trajectory $\alpha'_{\mathbb{P}}(0)$. Using the result (11) of this experiment one gets

$$\alpha'_{\mathbb{P}}(0) \sim 0.26 \text{ GeV}^{-2} ,$$

which is in good agreement with the value obtained by other methods [28]. This consistency check favours the description of the cluster production by the correlated cluster link model (CLM).

## 5. CONCLUSIONS

The data presented in this paper show:

(a) The charge compensation in non-diffractive events is due to a strong local and a weak global component.

(b) Particles of equal charge tend to be produced at small distances in phase space (Bose-Einstein effect).

(c) The transverse momenta of the produced particles are compensated over a range in rapidity which is comparable to the total rapidity range available.

For a quantitative description of these results, the full set of correlation data has been analyzed in the framework of cluster models with one set of parameters, which has been derived from the observed single and two-particle densities and the measured charge density. From the comparison of the model predictions with the data follows:

(a) The charge correlation data are best described by a cluster model with local charge exchange (LCEX). A model with independent emmision of neutral clusters (IENC) can be ruled out definitely, while a model assuming independent emission of charged clusters (IECC) shows small but significant deviations from the data only for the long range component.

(b) The predictions of the uncorrelated cluster jet model (UJM) and the correlated cluster link model (CLM) for the correlations of the transverse momenta are in good agreement with the data. The observed long range correlations are in disagreement with the predictions of the uncorrelated cluster link model (ULM).

(c) The mean transverse momentum of the produced cluster is $\langle k_T \rangle = (0.65 \pm 0.1)$ GeV/c. Using this result and the connection between the imaginary part of the elastic and the inelastic scattering amplitude as given by the cluster models, only the correlated cluster link model (CLM) is able to give an overall consistent description. In this framework the slope of the Pomeron trajectory is found to be

$$\alpha'_{\mathbb{P}}(0) \simeq 0.26 \text{ GeV}^{-2}.$$

(d) The Bose-Einstein correlations between particles of equal charge can be described as a second order interference phenomenon. A radius $R = (1.34 \pm 0.31)$ fm and a lifetime of $c\tau = (1.38 \pm 0.6)$ fm for the pion source are obtained.

Acknowledgement

This experiment was greatly helped by contributions from the SFM Detector group, in particular by W. Bell, E. Chesi, B. Heck, L. Naumann and F. Piuz. We are indebted to H.F. Hoffmann and the ISR experimental support group. For on-line programming, the contributions of M. Sciré were essential. We wish to thank U. Schlüpmann and the SFM software group for assistance and for development of the off-line programs. The Heidelberg and the Karlsruhe group have been supported by a grant from the Bundesministerium für Forschung und Technologie of the Federal Republic of Germany, the Collège de France group was funded by IN2P3 and the CEA.

APPENDIX A

RELATIONS BETWEEN PARTICLE AND CHARGE DENSITIES

For convenience, we collect here some relations between the particle and charge densities used in the present paper and those used in other analyses.

The associated particle density $\rho_n^{ab}(y_1|y_2)$ for a fixed multiplicity $n = n_+ + n_-$, i.e. the density of particles of charge a at rapidity $y_1$ under the condition that a particle of charge b was found at $y_2$, in an event of total charged multiplicity n, is related to the semi-inclusive two-particle density $\rho_n^{ab}(y_1,y_2)$

$$\rho_n^{ab}(y_1,y_2) = \rho_n^{ab}(y_1|y_2) \cdot \rho_n^{b}(y_2).$$

Using the relation

$$\int \rho_n^{ab}(y_1|y_2)\, dy_1 = n_a - \delta_{ab}$$

and averaging over all multiplicities one derives the sum rules

$$\begin{aligned} \int \left\{ \rho^{++}(y_1,y_2) - \rho^{-+}(y_1,y_2) \right\} dy_1 &= (Q-1)\rho^{+}(y_2) \\ \int \left\{ \rho^{+-}(y_1,y_2) - \rho^{--}(y_1,y_2) \right\} dy_1 &= (Q+1)\rho^{-}(y_2), \end{aligned} \qquad \text{(A.1)}$$

where $Q = n_+ - n_-$ is the total initial charge.

The associated charge density balance $\Delta q(y_1|y_2)$, as defined in sect. 3.1, can then be expressed in terms of two-particle densities as

follows:

$$\Delta q(y_1|y_2) = -\,(q(y_1|+,y_2) - q(y_1|-,y_2)) =$$

$$= -\left\{\frac{\rho^{++}(y_1,y_2) - \rho^{-+}(y_1,y_2)}{\rho^{+}(y_2)} - \frac{\rho^{+-}(y_1,y_2) - \rho^{--}(y_1,y_2)}{\rho^{-}(y_2)}\right\} \tag{A.2}$$

$$= \frac{C^{+-}(y_1,y_2) - C^{--}(y_1,y_2)}{\rho^{-}(y_2)} - \frac{C^{++}(y_1,y_2) - C^{-+}(y_1,y_2)}{\rho^{+}(y_2)}\,.$$

From this expression and the sum rule (A.1) one obtains the normalization

$$\int \Delta q(y_1|y_2)\,dy_1 = 2,$$

independent of $y_2$ and the initial charge Q.

In a very naive model of independent emission of positive and negative particles, taking only into account correlations due to charge conservation (as expressed by (A.1)), i.e. setting

$$\rho^{++}(y_1,y_2) = \frac{\langle n_+(n_+-1)\rangle}{\langle n_+\rangle^2}\,\rho^{+}(y_1)\,\rho^{+}(y_2), \text{ etc.},$$

one finds

$$\Delta q(y_1|y_2) = \alpha_-\rho^{-}(y_1) + \alpha_+\rho^{+}(y_1),$$

which is independent of $y_2$ ($\alpha_+$ and $\alpha_-$ are constants).

Another quantity which can be used to study charge correlations is the charge transfer correlation function [13,19]

$$D(y_1,y_2) = \langle U(y_1)U(y_2)\rangle - \langle U(y_1)\rangle\langle U(y_2)\rangle, \tag{A.3}$$

where U(y) is the charge transfer at rapidity y, defined for every event

$$U(y) = \sum_i Q_i \theta(y-y_i) - Q_a \theta(y-y_a) - Q_b \theta(y-y_b);$$

a, b characterize the initial particles (beam and target) and $Q_i$ is the charge of particle i at rapidity $y_i$. The average in (A.3) is taken over all events. $D(y_1,y_2)$ can be expressed by particle density correlation functions

$$D(y_1,y_2) = -\int_{\infty}^{y_1} dy \int_{y_2}^{\infty} dy' \left\{ C^{++}(y,y') - C^{+-}(y,y') - C^{-+}(y,y') + C^{--}(y,y') \right\}.$$

With the help of the sum rules (A.1) one finds

$$\frac{d^2D(y_1,y_2)}{dy_1\, dy_2} = \left\{ \rho^+(y_1) + \rho^-(y_1) \right\} \delta(y_1-y_2) + C^{++}(y_1,y_2) - C^{+-}(y_1,y_2) - C^{-+}(y_1,y_2) + C^{--}(y_1,y_2) .$$

More information can be found in refs [1] (paper by Bopp), [3] and [13].

APPENDIX B

## DETAILS OF MODEL CALCULATION

### B.1 Free parameters of the cluster model

As described in sect. 4.1, the width $\delta$ of cluster decay and the strength F of the short-range correlation are obtained from a fit to the correlation function $C'(y|0)$. From the analysis of semi-inclusive correlations [1,3,4] it is known that the charged multiplicity distribution of cluster decay is narrower than a Poisson-distribution. Therefore the average charged multiplicity $\langle\kappa\rangle$ of cluster decay fulfills the inequality

$$1.24 \leqslant \langle\kappa\rangle \leqslant 2.24,$$

where the lower limit corresponds to a Poisson and the upper limit to a $\delta$-like multiplicity distribution(*). For a Poisson-distribution with $\bar{n} = 1.24$, the probability $p(n)$ for $n \geqslant 4$ is small ($p(4) \sim 0.03$, $p(5) \sim 7 \cdot 10^{-3}$). Therefore cluster decays into more than four charged particles are neglected. Since we limit ourselves to neutral and singly charged clusters (isospin = 1), the following numbers of charged decay products are possible: 0, 2, 4 for neutral clusters and 1, 3 for charged clusters. If we denote by $W_Q(\kappa)$ the probability for a cluster of charge $Q(Q = 0, \pm 1)$ to decay into $\kappa$ charged particles (plus any number of neutrals), we are left with five unknowns which are constrained by the relations

$$W_1(1) + W_1(3) = 1$$

$$W_o(0) + W_o(2) + W_o(4) = 1.$$

Following ref. [4], we set $W_o(0) = 0.1$. Assuming the strength F of the short range correlation to be the same for neutral and charged clusters one obtains the parameters of the cluster decay multiplicity distribution

---

(*) Note that $F + 1 = \langle\kappa\rangle + (\langle\kappa^2\rangle - \langle\kappa\rangle^2)/\langle\kappa\rangle$.

from the relation

$$F = \frac{\langle \kappa(\kappa-1) \rangle}{\langle \kappa \rangle} = \frac{\Sigma W(\kappa)\kappa(\kappa-1)}{\Sigma W(\kappa)\kappa} \quad .$$

The resulting values are

$$W_o(2) = 0.85 \qquad W_o(4) = 0.05$$

$$W_1(1) = 0.65 \qquad W_1(3) = 0.35,$$

corresponding to $\langle \kappa \rangle \simeq 1.9$ for neutral and $\langle \kappa \rangle \simeq 1.7$ for charged clusters. Since there are indications [4] that the number of neutral clusters is about the same as that of charged clusters, and since the two values agree within the uncertainties of their determinations, we use $\langle \kappa \rangle \sim 1.8$ for all clusters, independent of their charge. From this and the measured value of the fully inclusive (i.e. without the restriction $n \gtrsim \langle n \rangle$) particle density, $\rho(0) \sim 1.8$, we obtain $\rho_C \sim 1$.

B.2 Model calculation and Monte-Carlo program

To calculate the predictions of the different cluster models described in sect. 3.2, a Monte-Carlo program was used, which agrees in its basic features with that of Arneodo and Plaut [4]. The relevant formulae of the model are collected in table 2, and table 3 contains the values of the free parameters of the model. Their determination is discussed in sect. 4 in connection with the presentation and interpretation of the data, and some additional information is given in the previous sect. (B.1).

For completeness, we present here a short summary of the model calculation. For details, refs [4] and [5] should be consulted.

The two leading clusters are generated with a uniform x-distribution ($x = 2p_L/\sqrt{s}$), with masses $M_L$ derived from the mass distribution in table 2. Their charges $Q_L$ are drawn in the set $\{0,1\}$ with probabilities $p_o = P(Q_L = 0)$ and $p_1 = P(Q_L = 1) = 1-p_o$. Different values of the mean charge have been tried in the range $\langle Q_L \rangle = p_1 \in [0.65,1]$; the model predictions are not very sensitive to the precise values.

The central clusters follow a uniform y-distribution, with density $\rho_C$, in a rapidity interval $y \in [y_C - \frac{1}{2} Y_{eff}, y_C + \frac{1}{2} Y_{eff}]$ (table 2), and their masses follow a distribution analogous to that of leading clusters. Energy and momentum conservation (to within $\sim$ 1%) is achieved by a boost of the central cluster system and an overall scaling of the energies of the central clusters. The charges $Q_C$ of the central clusters are selected from the set $\{-1,0,+1\}$ with equal probabilities 1/3, subject to overall charge conservation. In the case of the LCEX, the charges are further constrained by the requirement that the charge exchange $\Delta Q$ between clusters adjacent in y (including leading clusters) is limited to the values -1,0,+1 [4,17,29].

Only for the study of transverse momentum correlations is the transverse momentum of clusters taken into account. In this case, the decay products of the clusters are generated according to phase-space (constant matrix element), in particular they are isotropic in the cluster rest frame.

To take into account the Bose-Einstein effect for pairs of like-charged particles, the weight factor $g_{BE}$ (given in table 2) is attached to each event.

The acceptance of the detector and the efficiency of the program chain is simulated by rejecting some of the generated tracks on the basis of our knowledge of the track acceptance, and events are accepted when they fulfill the selection criterion $n_{obs} \geq 7$. When relevant, the same cuts are applied to simulated and real data (e.g. $p_T > 0.1$ GeV/c for transverse momentum correlations). All cuts applied, the predicted multiplicity distribution agrees with the observed one for the full range of $n_{obs}$.

REFERENCES

[1] J. Whitmore, Phys. Report 10C (1974) 273;

L. Foà, Phys. Report 22C (1975) 1;

M. Le Bellac, Rapp. talk, Budapest Conf. 1977, preprint CERN/TH 2361, August 1977;

F.W. Bopp, The Cluster Model, Siegen preprint SI-77-4 (1977) and further ref. quoted in these papers.

[2] E.L. Berger, Phys. Lett. 49B (1974) 369;

E.L. Berger, Nucl. Phys. B85 (1975) 61.

[3] M. Le Bellac, Yellow Report CERN 76-14 (1976).

[4] A. Arneodo and G. Plaut, Nucl. Phys. B107 (1976) 262;

A. Arneodo and G. Plaut, Nucl. Phys. B113 (1976) 156.

[5] W. Hofmann, Thesis Karlsruhe 1977, Kernforschungszentrum Karlsruhe, Report KfK 2489 (1977).

[6] R. Bouclier et al., Nucl. Instr. and Meth. 115 (1974) 235.

[7] R. Bouclier et al., Nucl. Instr. and Meth. 125 (1975) 19.

[8] CCHK Collaboration, M. Della Negra et al., Nucl. Phys. B127 (1977) 1.

[9] W. Bell et al., Nucl. Instr. and Meth. 125 (1975) 437.

[10] H. Grote, M. Metcalf, C. Onions, F. Ranjard, A. User's guide to the SFM off-line program chain, CERN OM Dev. Note AP-18 (1976);

A. Fröhlich, H. Grote, C. Onions, F. Ranjard, MARC - Track finding in the split field magnet facility, report CERN/DD 76-5 (1976);

A. Metcalf, M. Regler, C. Broll, A split field magnet geometry program "NICOLE", Yellow Report CERN 73-2 (1973).

[11] W. Thomé et al., Nucl. Phys. B129 (1977) 365.

[12] See e.g. lectures by Z. Koba at the 1973 CERN-JINR School of Physics, Ebeltoft, Yellow Report CERN 73-12 (1973).

[13] A. Krzywicki, Nucl. Phys. B86 (1975) 296;

D. Weingarten, Phys. Rev. D11 (1975) 1924.

[14] L. van Hove and S. Pokorski, Acta Phys. Polonica B5 (1974) 229.

REFERENCES (Cont'd)

[15] L. van Hove, Rev. Mod. Phys. 36 (1964) 655;
A. Bassetto, M. Toller, L. Sertorio, Nucl. Phys. B34 (1971) 1.

[16] F. Henyey, Phys. Lett 45B (1973) 469;
J.L. Meunier and G. Plaut, Nucl. Phys. B87 (1975) 74.

[17] J. Kubar-André, M. Le Bellac and J. Meunier, Nucl. Phys. B93 (1975) 138;
C. Michael, Nucl. Phys. B103 (1976) 296.

[18] C. Quigg and G.H. Thomas, Phys. Rev. D7 (1973) 2752.

[19] P. Pirilä, G. Thomas and C. Quigg, Phys. Rev. D12 (1975) 92.

[20] See e.g. P. Darriulat, Rapp. talk, 6th Inter. symposium on multiparticle reactions, Oxford 1975.

[21] T. Kafka et al., Phys. Rev. D16 (1977) 1261.

[22] G.I. Kopylov and M.I. Podgoretskii, Sov. Journ. Phys. 19 (1974) 434;
G.I. Kopylov and M.I. Podgoretskii, Sov. Journ. Phys. 18 (1973) 656;
G.I. Kopylov, Phys. Lett. 50B (1974) 472 and earlier papers quoted in these publications.

[23] G. Cocconi, Phys. Lett. 49B (1974) 459.

[24] M. Deutschmann et al., A study of the Bose-Einstein interference for pions produced in various hadronic interactions, CERN/EP/PHYS 78-1 (1978) and references quoted therein.

[25] F. Hayot, F.S. Henyey and M. Le Bellac, Nucl. Phys. B80 (1974) 77.

[26] A. Arneodo and J.L. Meunier, Cluster models, local compensation of transverse momenta and transverse data, Univ. of Nice preprint N TH 78/2 March 1978.

[27] H. Kirk et al., Nucl. Phys. B128 (1977) 397.

[28] H.J. Behrend et al., Phys. Lett. 56B (1975) 408;
D.S. Ayres et al., Phys. Rev. D15 (1977) 3105;
H.J. Behrend et al., DESY 78/26 (1978).

[29] P. Grassberger, C. Michael and H. Miettinen, Phys. Lett. 52B (1974) 60.

TABLE CAPTIONS

Table 1 Definition of kinematical variables and experimental distributions.

Table 2 Variables, parameters and formulae of the cluster model.

Table 3 Values and method of determination of the free parameters of the cluster model.

Table 1

| | | |
|---|---|---|
| Longitudinal momentum | $p_L$ | Defined in the proton-proton centre of mass system |
| Feynman variable | $x = \frac{2p_L}{\sqrt{s}}$ | |
| Rapidity | $y$ | |
| Transverse momentum | $p_T$ | |
| Transverse mass | $m_T^2 = (p_T^2 + m^2)$ | |
| Azimuthal angle | $\phi$ | |
| Particle density | $\rho(y) = \frac{1}{\sigma}\frac{d\sigma}{dy}$ | |
| Charge density | $q(y) = \rho^+(y) - \rho^-(y)$ | upper index refers to particle charge |
| Two-particle density | $\rho_2(y_1,y_2) = \frac{1}{\sigma}\frac{d^2\sigma}{dy_1 dy_2}$ | |
| Correlation function | $C(y_1,y_2) = \rho_2(y_1,y_2) - \rho(y_1)\cdot\rho(y_2)$ | |
| Normalized correlation function | $R'(y_1,y_2) = \alpha\frac{\rho_2(y_1,y_2)}{\rho(y_1)\rho(y_2)} - 1$ | $\alpha = 1$ non-identical particles<br>$\alpha = \frac{\langle n^2\rangle}{\langle n(n-1)\rangle}$ identical particles |
| Conditional correlation function | $C'(y_1\|y_2) = C(y_1,y_2)/\rho(y_2) = \rho(y_1\|y_2) - \rho(y_1)$ | |

Table 2

| | |
|---|---|
| Transverse momentum distribution of clusters | $dN/dk_T^2 \sim \exp(-k_T^2/\langle k_T^2\rangle)$ |
| Transverse mass of central clusters | $M_T$ |
| Charged cluster decay multiplicity | $\kappa$ |
| Distribution function of $\kappa$ | $w(\kappa)$ (see Appendix B) |
| Strength of short-range correlations | $F = \langle\kappa(\kappa-1)\rangle/\langle\kappa\rangle$ |
| Density of decay particles in cluster rest frame | $dN/dy = (\kappa/\delta\sqrt{2\pi})\exp(-y^2/2\delta^2)$ |
| Matrix element for cluster decay | $M_{fi}$ = const. (decay according to phase-space weights) |
| Bose-Einstein weight factor | $g_{BE} = \prod_{\substack{i,j=1 \\ i<j}}^{n}\left[1+\delta(Q_i-Q_j)\delta(m_i-m_j)\exp(-(\vec{p}_i-\vec{p}_j)^2/2\varepsilon^2)\right]$<br>Q, m charge and mass of particle<br>n = total multiplicity |
| x of leading clusters | $x_1$, $x_2$ |
| Mean charge of leading clusters | $\langle Q_L\rangle > 0$ |
| Mass distribution of leading clusters | $w(M) = (M-M_o)\exp\left[-(M-M_o)/M_1\right]$; $\langle M_L\rangle = 2M_1+M_o$ |

Table 2 (Cont'd)

| | |
|---|---|
| Effective mass of central cluster system | $W_C^2 = s(1-x_1)(1-x_2)$ |
| Distribution function of central cluster masses | $W(M) = (M-M_2)\exp\left[-(M-M_2)/M_3\right]$; $\langle M_C \rangle = 2M_3+M_2$ |
| Density $\frac{dn}{dy}$ of central clusters | $\rho_C$ |
| Rapidity width of central cluster system | $Y_{eff} = \ln W_C^2 - \ln(\rho_C M_T)^2$ |
| Mean rapidity of central system | $y_C = \frac{1}{2} \ln\left(\frac{1-x_1}{1-x_2}\right)$ |
| Number of central clusters | Poisson distributed $\langle n_C \rangle = Y_{eff} \rho_C$ |
| Charge of central clusters | IENC $Q_C = 0,1$ |
| | IECC $Q_C = -1,0,1$; $W(Q_C) = 1/3$ |
| | LCEX $Q_C = -1,0,1$; $W(Q_C)$ defined by assumption of isospin 1 clusters and links [4]. |
| Mean total charge of central clusters | $\langle \Sigma Q_C \rangle = 2(1 - \langle Q_L \rangle)$ |

Table 3

| Parameter | Value | Determined from |
|---|---|---|
| Mass parameters of leading cluster | $\langle M_L \rangle = 1.5$ GeV | position in y of maximum of q(y) (fig. 2) |
| | $M_0 = 1$ GeV | assumption |
| Mean charge of leading cluster | $\langle Q_L \rangle \geq 0.65$ | shape of q(y) (fig. 2) |
| Density in y of central clusters | $\rho_C \simeq 1$ | $\rho(y)$ and $\langle \kappa \rangle$ (fig. 2) |
| Decay multiplicity of central clusters | $\langle \kappa \rangle = 1.8$ | F (fit to $C'(y\|0)$) (fig. 3(a)) |
| Decay width of central cluster | $\delta = 0.65$ | fit to $C'(y\|0)$ (fig. 3(a)) |
| Transverse momentum of central cluster | $\langle k_T \rangle = 0.65$ GeV/c | average compensating transverse momentum (fig. 12) |
| Mass parameter of central cluster | $\langle M_C \rangle = 1.3$ GeV | relation between $\langle k_T \rangle$, $\langle \kappa \rangle$ and $\langle p_T \rangle$ of produced particles ($\langle p_T \rangle \simeq 0.35$ GeV/c, [5][25] |
| | $M_2 = 0.3$ GeV | assumption |
| Correlation length for Bose-Einstein effect | $\varepsilon = 0.15$ GeV/c | fit to fig. 10(b) |

FIGURE CAPTIONS

Fig. 1 Kinematics of cluster production; $\vec{k}_i$ are the momenta of the clusters, $\vec{q}_i$ is the momentum exchanged between clusters i and i+1 which are ordered according to their rapidity $y_i > y_{i+1}$.

Fig. 2 Particle density $\rho(y)$ and charge density $q(y)$ for events with an observed charged multiplicity $n_{obs} \geq 7$. The charge density is normalized to 2. The full lines are the predictions of a cluster model with independent emission of charged clusters (IECC).

Fig. 3 Two-particle correlation function $C'(y_1|y_2) = C(y_1,y_2)/\rho(y_2) = \rho(y_1|y_2) - \rho(y_1)$ as a function of $y_1$, for different values of $y_2$: (a) $y_2 = 0$, (b) $y_2 = -2$, (c) $y_2 = -4$. The lines are the predictions of a cluster model with independent emission of charged cluster (IECC).

Fig. 4 Associated charge density balance $\Delta q(y_1|y_2)$ as a function of $y_1$, for different values of $y_2$: (a) $y_2 = 0$, (b) $y_2 = -1$, (c) $y_2 = -2$, (d) $y_2 = -3$. For comparison, also the associated particle density $\rho(y_1|y_2)$ is shown (broken lines).

Fig. 5 Charge density balance $\Delta q(y_1|y_2)$ associated with a central particle ($|y_2| \leq 1$) as a function of $\Delta y = |y_1-y_2|$. Also shown are the predictions of the IENC, IECC and LCEX models.

Fig. 6 Charge density balance $\Delta q(y_1|y_2)$ associated with a particle at $y_2 = -2$, as a function of $y_1$. The curves represent the predictions of the IENC (dotted), IECC (dashed) and LCEX (full line) models.

FIGURE CAPTIONS (Cont'd)

Fig. 7 Charge density balance $\Delta q(y_1,\phi_1|y_2,\phi_2)$ associated with a central particle ($|y_2| < 1.5$) as a function of $\Delta y = |y_1-y_2|$ and $\Delta\phi = |\phi_1-\phi_2|$, for two different regions of the transverse momentum $p_{T2}$ of the selected particle: (a) $p_{T2} > 0.1$ GeV/c, (b) $p_{T2} > 0.5$ GeV/c.

Fig. 8 Normalized two-particle correlation function $R'(y_1,\phi_1;y_2,\phi_2)$ as a function of $\Delta y = |y_1-y_2|$ and $\Delta\phi = |\phi_1-\phi_2|$. Only particles with $p_T > 0.2$ GeV/c and $|y| < 2.5$ are taken into account: (a) pairs of particles with opposite charge, (b) pairs of particles with equal charge.

Fig. 9 Definition of $q_L$ and $q_T$ for a pair of particles with momenta $\vec{p}_1,\vec{p}_2$.

Fig. 10 Normalized two-particle correlation function $R'(\vec{p}_1,\vec{p}_2)$ for like (full circles) and unlike (open circles) charged particles. The full lines show the results of the fit with formulae (10): (a) $R'(\vec{p}_1,\vec{p}_2)$ vs $q_T$ for $q_L \leq 0.1$ GeV/c, (b) $R'(\vec{p}_1,\vec{p}_2)$ vs $q_L$ for $q_T \leq 0.2$ GeV/c.

Fig. 11 Associated compensating transverse momentum density $\Pi_T(y_1|y_2)$ vs $y_1$, for different values of $y_2$: (a) $y_2 = 0$, (b) $y_2 = -1$, (c) $y_2 = -2$, (d) $y_2 = -3$. For comparison, also the associated particle density $\rho(y_1|y_2)$ (dashed line) and the associated charge density balance $\Delta q(y_1|y_2)$ (dashed-dotted line) are shown.

Fig. 12 Average compensating transverse momentum $\pi_T(y_1|y_2)$ vs $\Delta y = |y_1-y_2|$, for $|y_2| \leq 1$, for different intervals in the transverse momentum $p_{T2}$ of the selected particle $h_2$: (a) the two hadrons $h_1,h_2$ have equal charge, (b) the two hadrons $h_1,h_2$ have opposite charge. The full line represents the prediction of the UJM with a cluster transverse momentum $\langle k_T \rangle = 0.65$ GeV/c (Bose-Einstein effects are included).

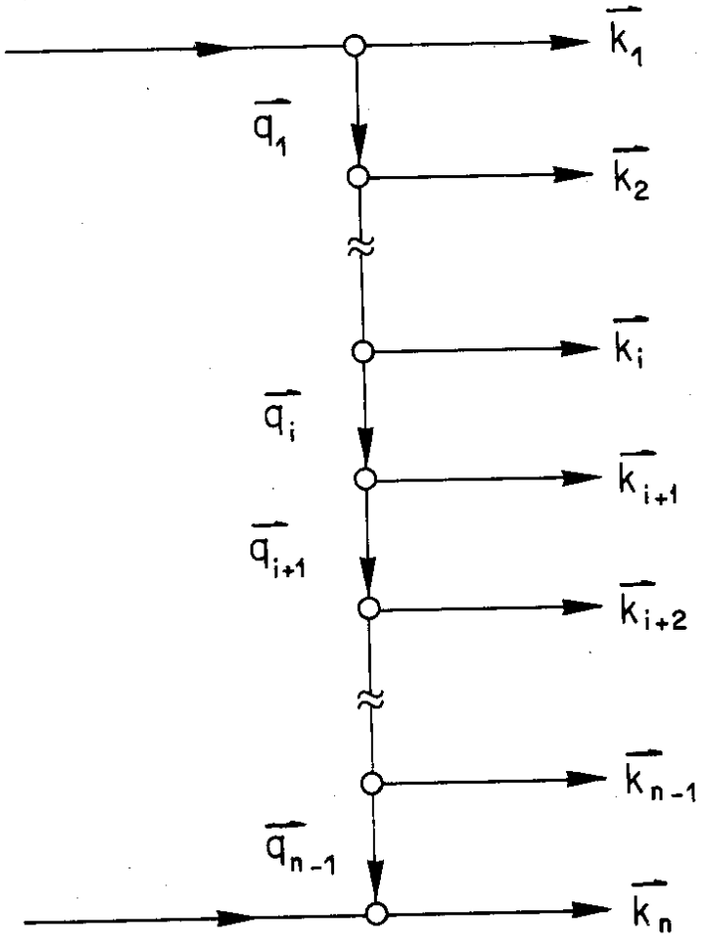
$\overrightarrow{k_1}$
$\overrightarrow{q_1}$
$\overrightarrow{k_2}$
$\overrightarrow{k_i}$
$\overrightarrow{q_i}$
$\overrightarrow{k_{i+1}}$
$\overrightarrow{q_{i+1}}$
$\overrightarrow{k_{i+2}}$
$\overrightarrow{k_{n-1}}$
$\overrightarrow{q_{n-1}}$
$\overrightarrow{k_n}$

Fig. 1

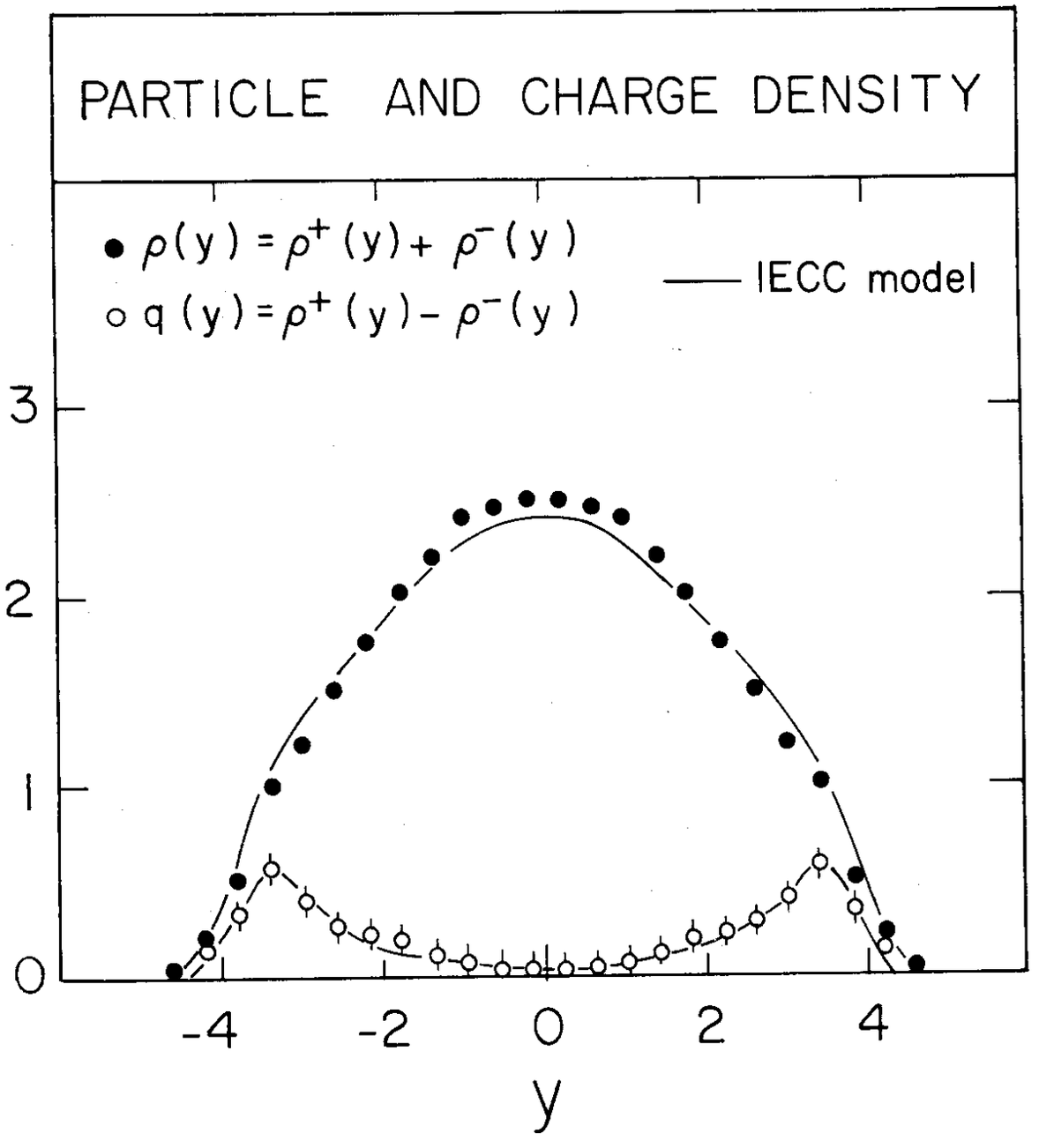
PARTICLE AND CHARGE DENSITY
● ρ(y) = ρ+(y) + ρ−(y)
○ q(y) = ρ+(y) − ρ−(y)
—— IECC model
3
2
1
0
-4
-2
0
2
4
y

Fig. 2

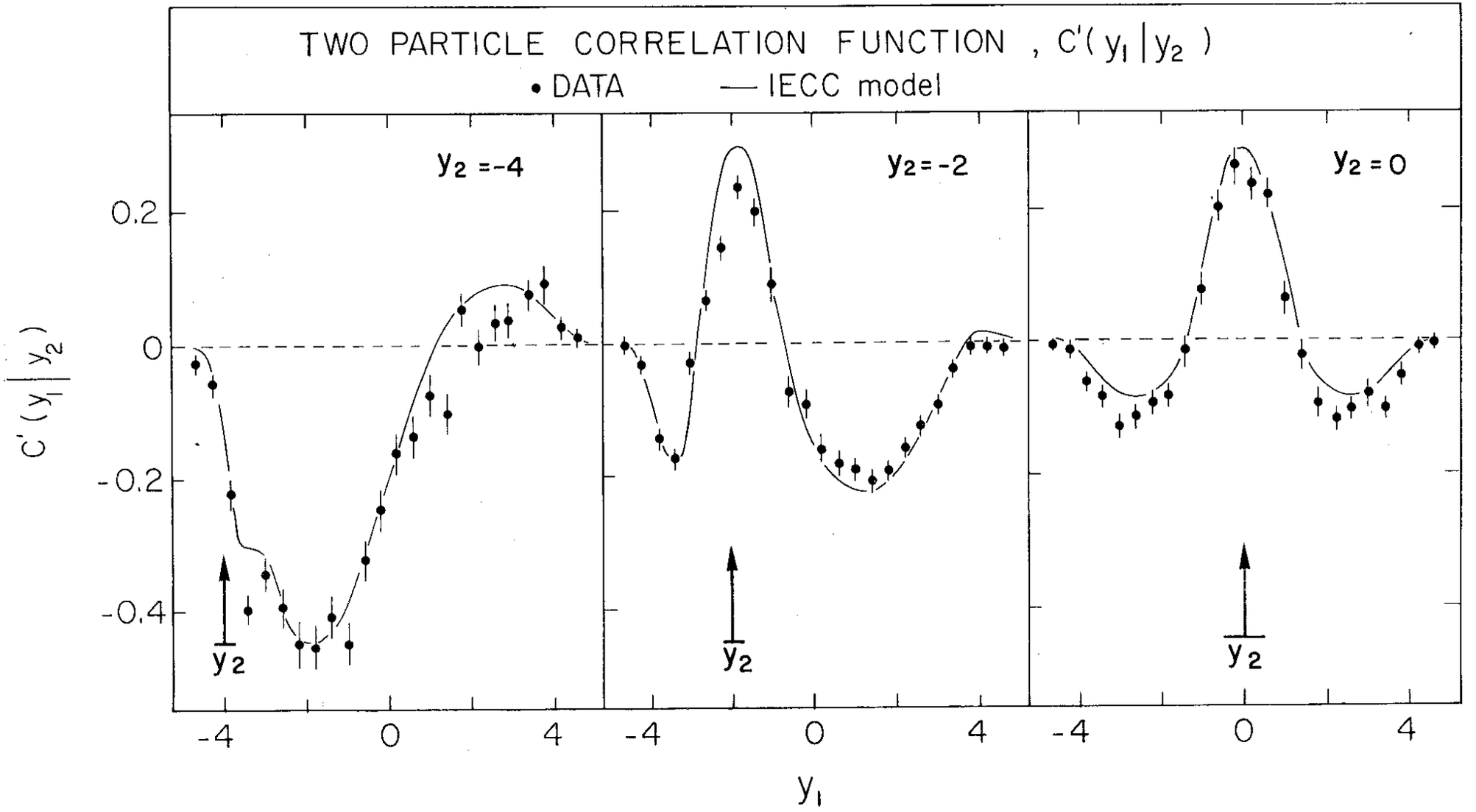
TWO PARTICLE CORRELATION FUNCTION , C'( y1 | y2 )
• DATA — IECC model
y2 =-4
y2=-2
y2 = 0
0.2
0
-0.2
-0.4
C' (y1 | y2)
y2
y2
y2
-4
0
4
-4
0
4
-4
0
4
y1

fig. 3

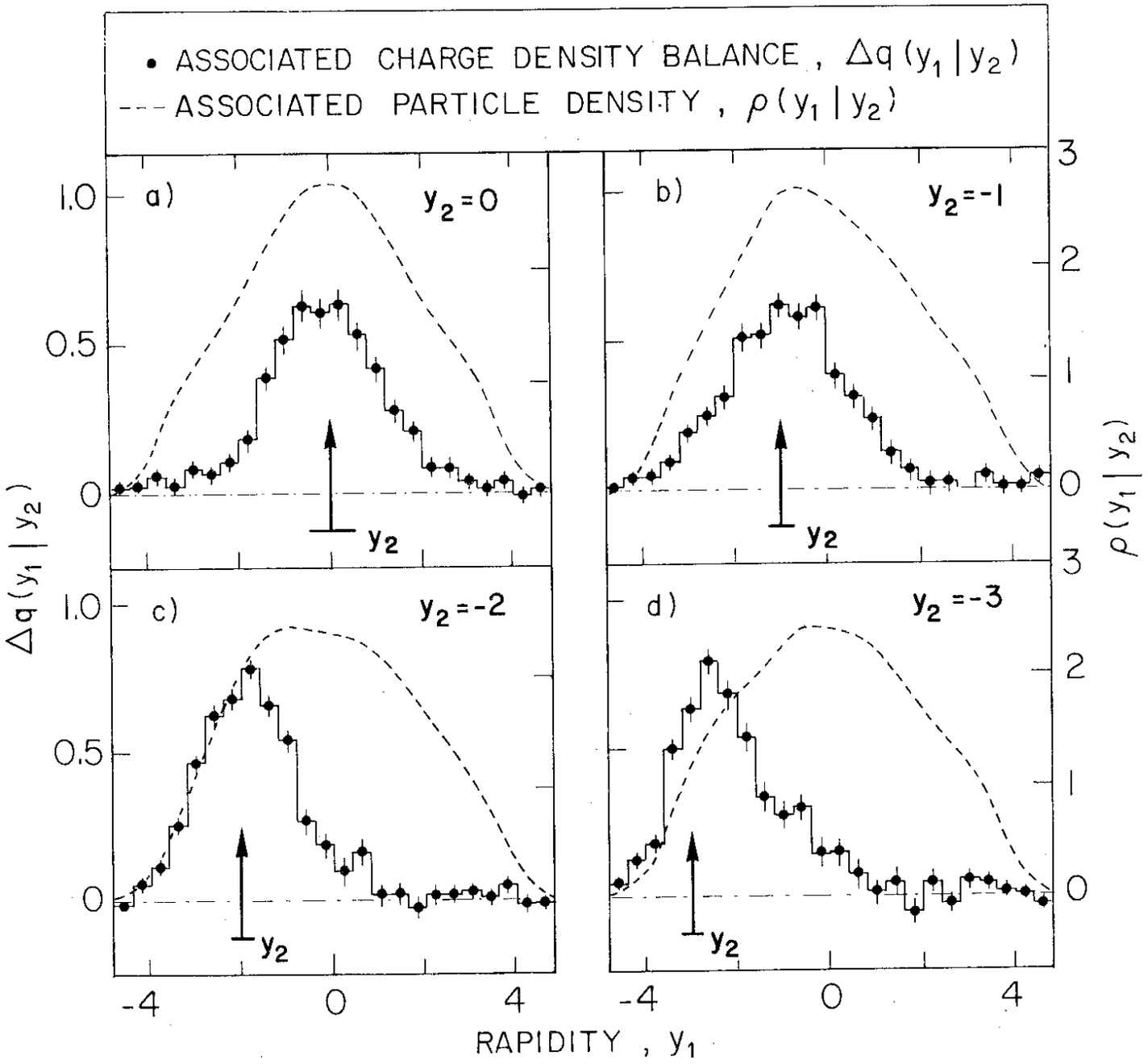
• ASSOCIATED CHARGE DENSITY BALANCE , Δq (y1 | y2)
--- ASSOCIATED PARTICLE DENSITY , ρ (y1 | y2)
a)
y2 = 0
b)
y2 = -1
c)
y2 = -2
d)
y2 = -3
y2
1.0
0.5
0
3
2
1
-4
0
4
Δq (y1 | y2)
ρ (y1 | y2)
RAPIDITY , y1

Fig. 4

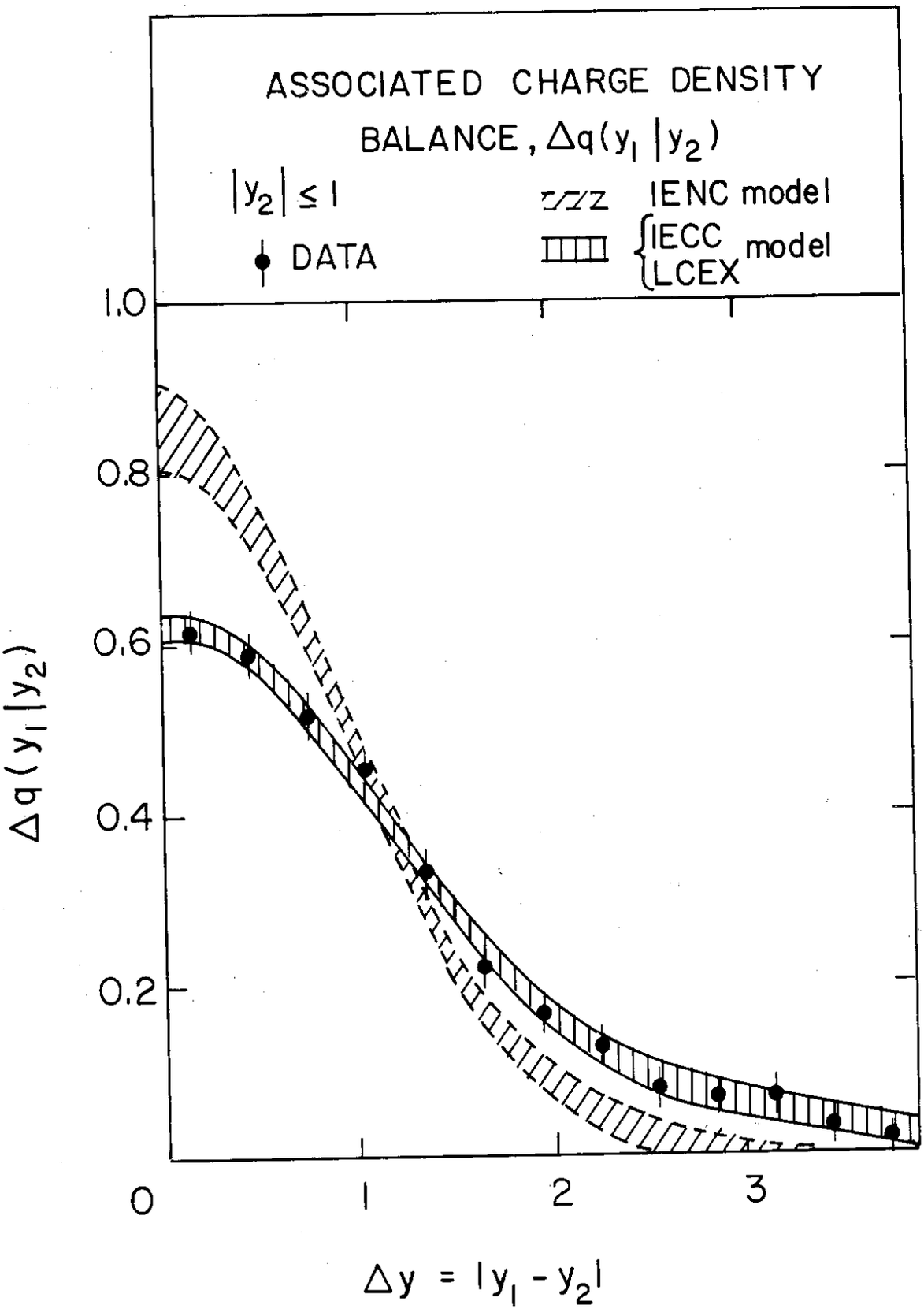
ASSOCIATED CHARGE DENSITY
BALANCE, Δq(y1 |y2)
|y2| ≤ 1
DATA
IENC model
IECC
LCEX
model
1.0
0.8
0.6
0.4
0.2
0
1
2
3
Δq(y1 |y2)
Δy = |y1 - y2|

Fig. 5

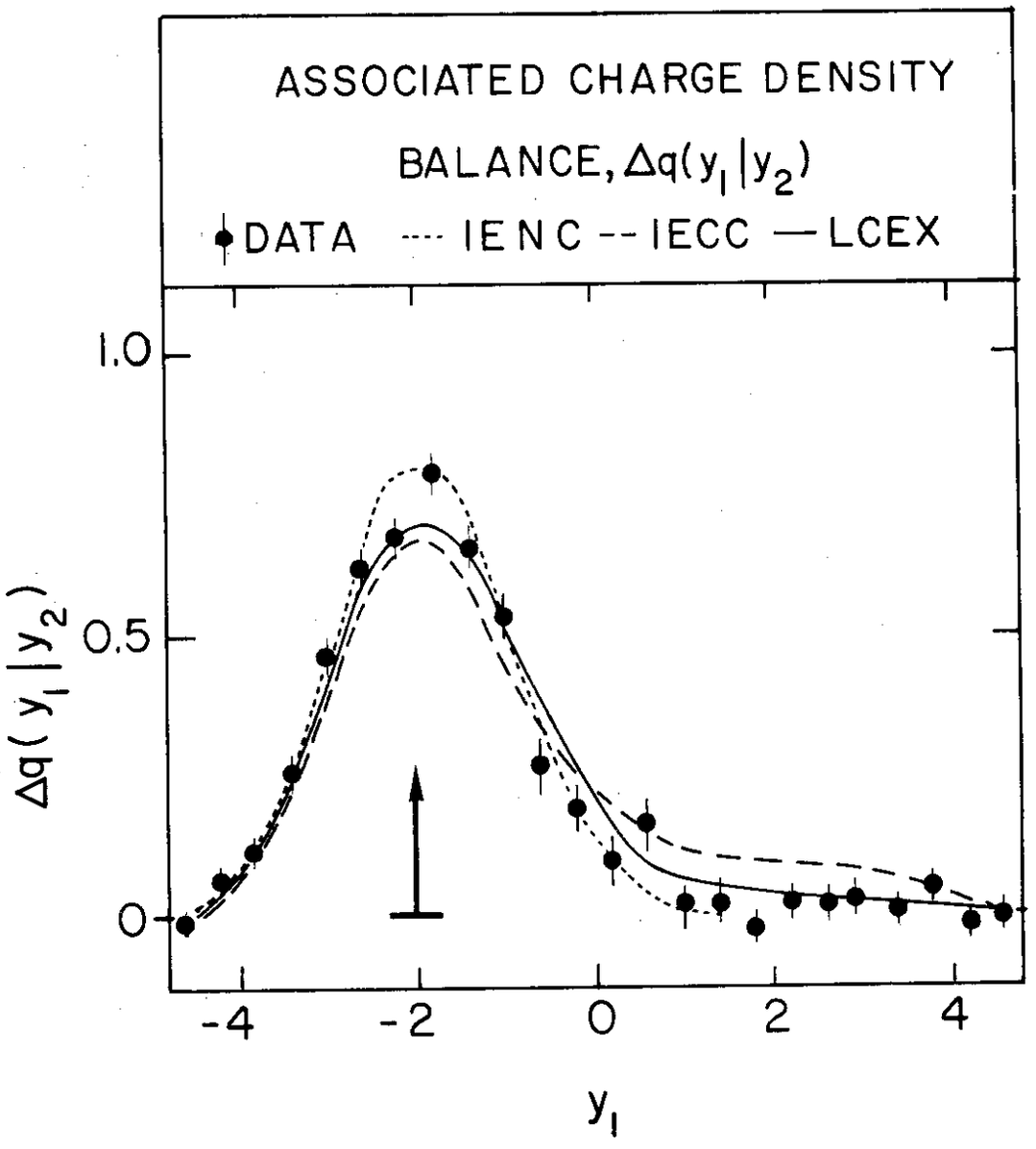
ASSOCIATED CHARGE DENSITY
BALANCE, Δq(y1|y2)
DATA
IENC
IECC
LCEX
1.0
0.5
0
Δq(y1|y2)
-4
-2
0
2
4
y1

Fig. 6

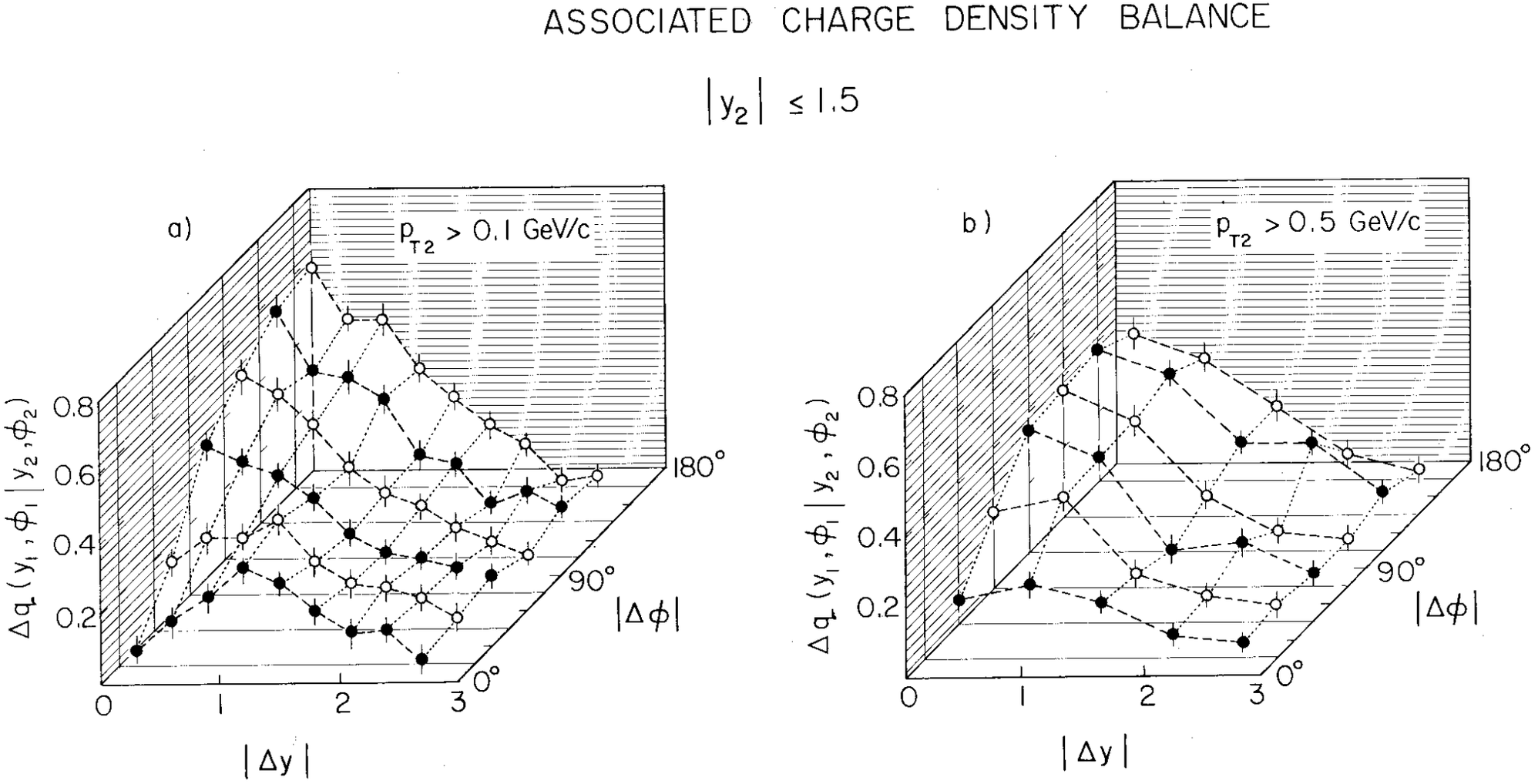
ASSOCIATED CHARGE DENSITY BALANCE
$|y_2| \leq 1.5$
a)
$p_{T2} > 0.1$ GeV/c
b)
$p_{T2} > 0.5$ GeV/c
$\Delta q(y_1, \phi_1 | y_2, \phi_2)$
0.8
0.6
0.4
0.2
0
1
2
3
$|\Delta y|$
0°
90°
180°
$|\Delta \phi|$

Fig. 7

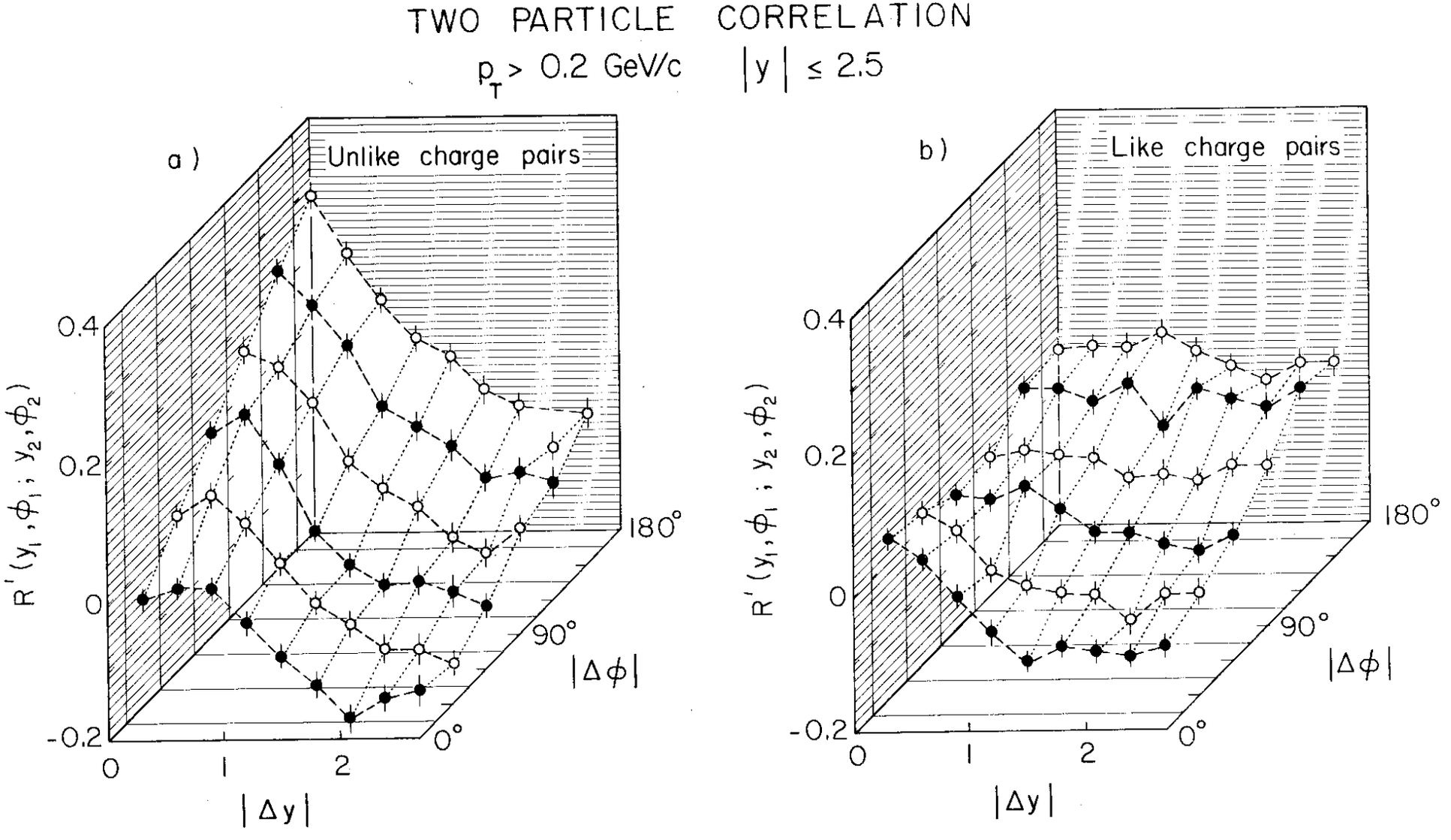
TWO PARTICLE CORRELATION
$p_T > 0.2$ GeV/c $|y| \leq 2.5$
a) Unlike charge pairs
b) Like charge pairs
$R'(y_1, \phi_1 ; y_2, \phi_2)$
0.4
0.2
0
-0.2
0
1
2
$|\Delta y|$
0°
90°
180°
$|\Delta \phi|$

Fig.8

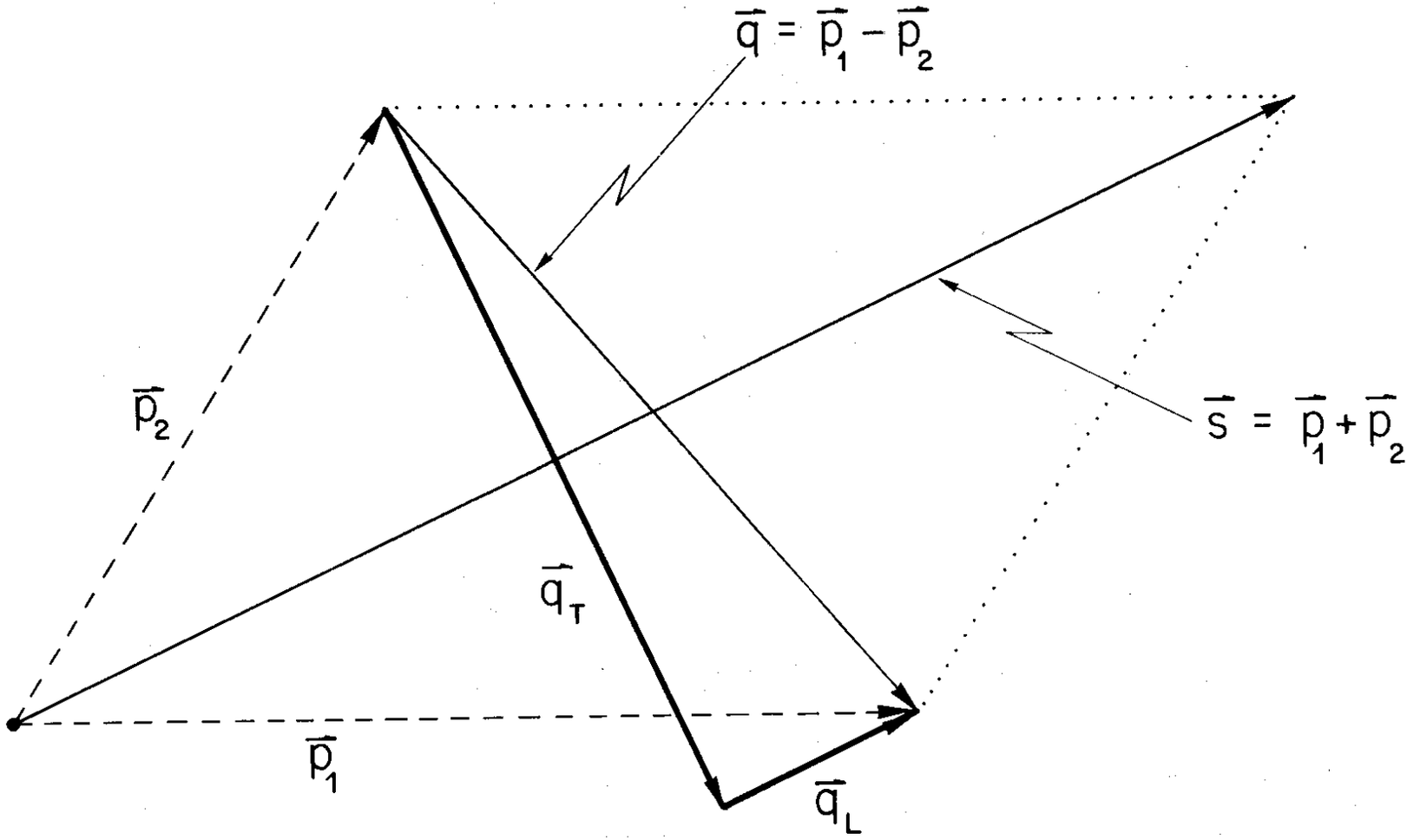


Fig. 9

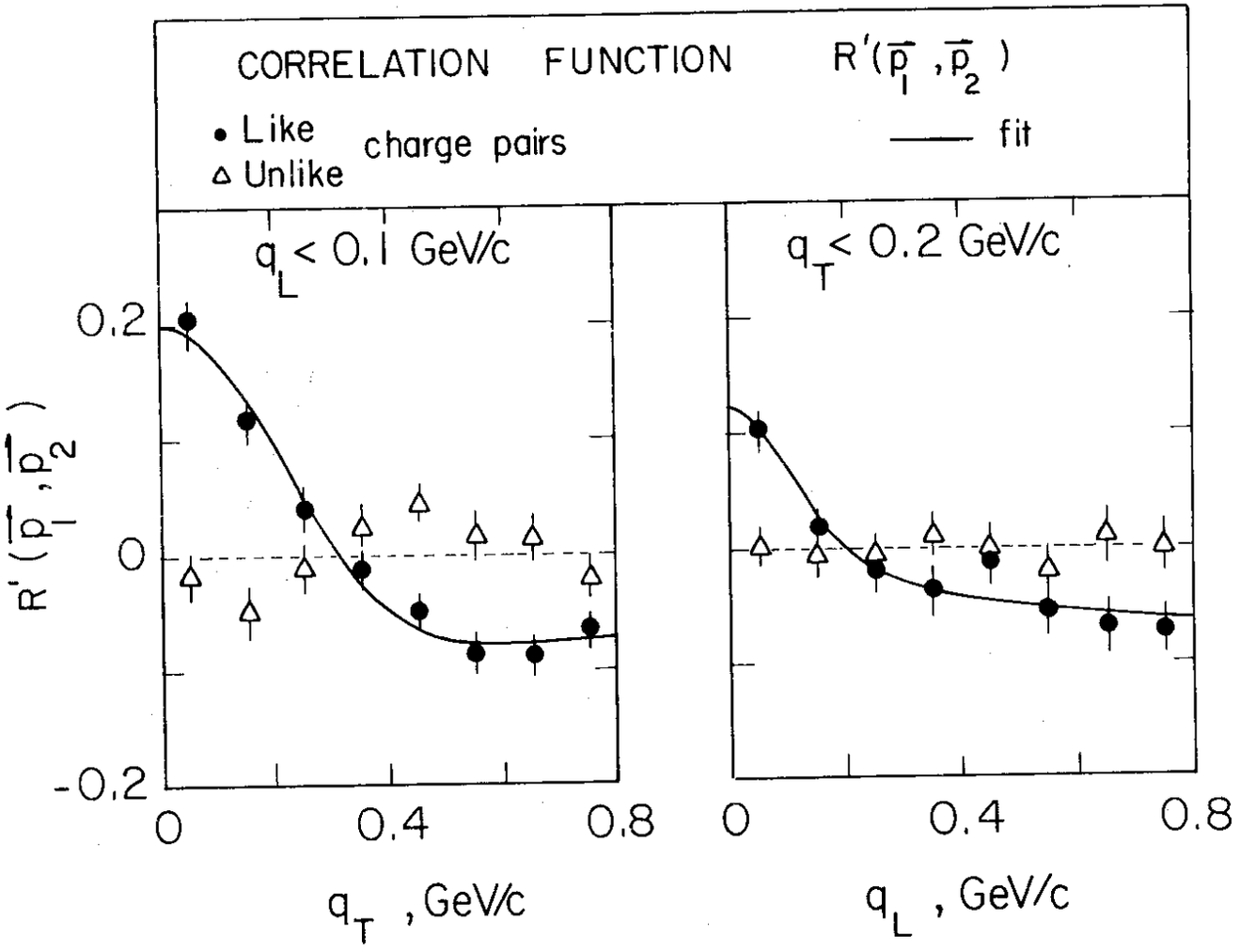
CORRELATION FUNCTION R'(p1 , p2 )
• Like charge pairs
△ Unlike
fit
qL < 0.1 GeV/c
qT < 0.2 GeV/c
0.2
0
-0.2
R'(p1 , p2 )
0
0.4
0.8
qT , GeV/c
qL , GeV/c

Fig.10

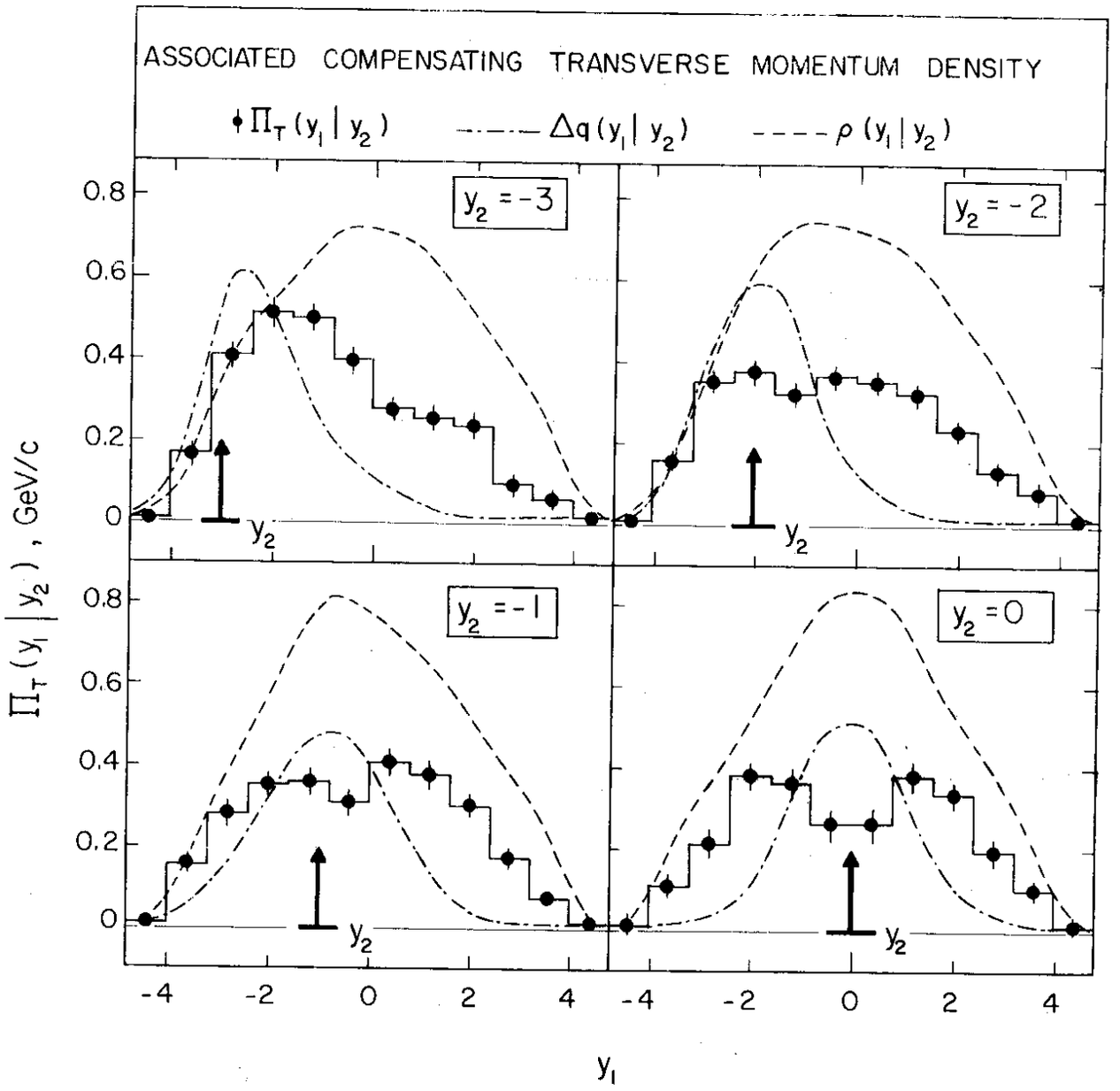
ASSOCIATED COMPENSATING TRANSVERSE MOMENTUM DENSITY
$\Pi_T(y_1 \mid y_2)$
$\Delta q(y_1 \mid y_2)$
$\rho(y_1 \mid y_2)$
$y_2 = -3$
$y_2 = -2$
$y_2 = -1$
$y_2 = 0$
$y_2$
$\Pi_T(y_1 \mid y_2)$, GeV/c
$y_1$
0.8
0.6
0.4
0.2
0
-4
-2
0
2
4

Fig.11

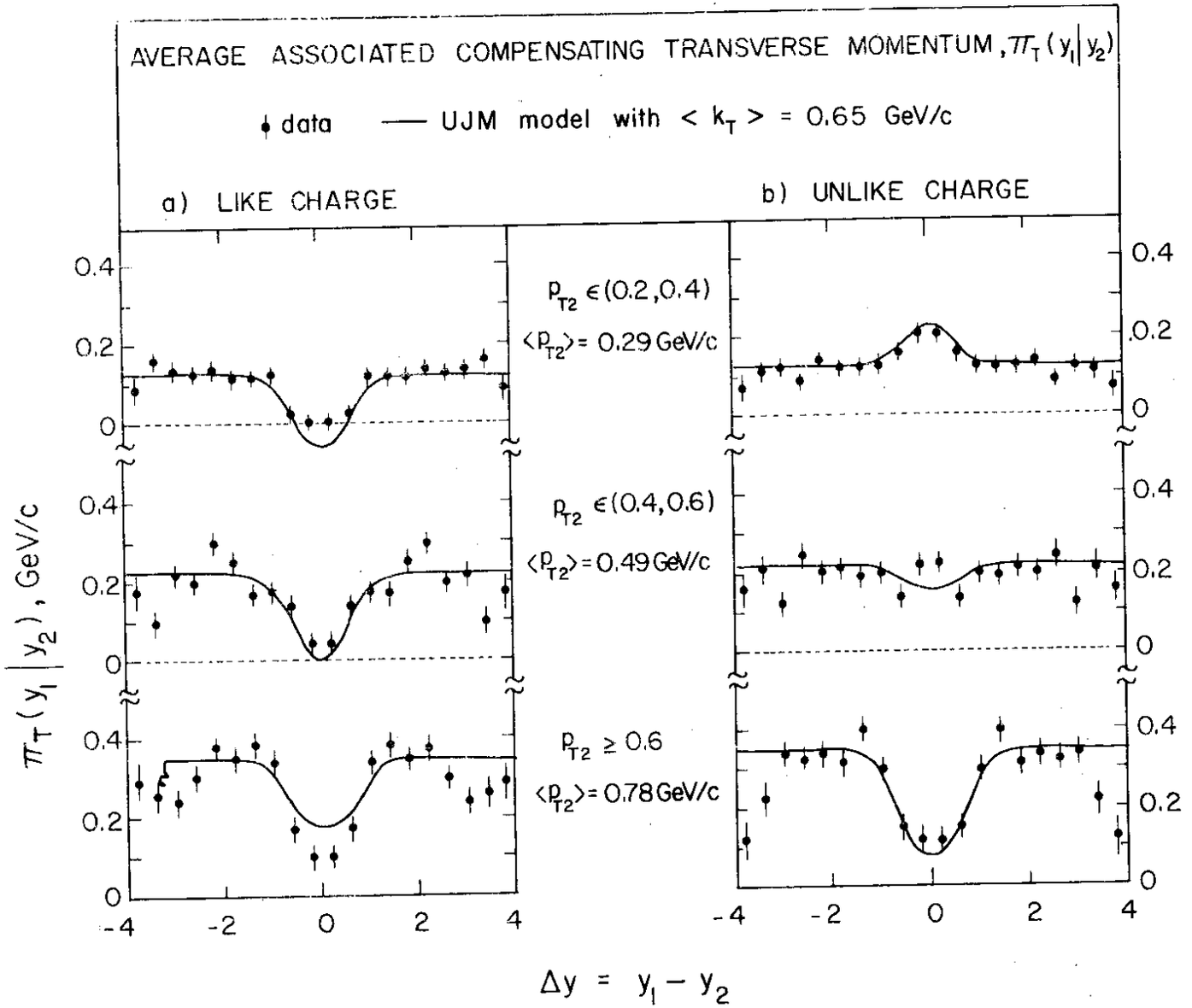
AVERAGE ASSOCIATED COMPENSATING TRANSVERSE MOMENTUM, $\pi_T(y_1|y_2)$
data
UJM model with $< k_T > = 0.65$ GeV/c
a) LIKE CHARGE
b) UNLIKE CHARGE
$p_{T2} \in (0.2, 0.4)$
$\langle p_{T2} \rangle = 0.29$ GeV/c
$p_{T2} \in (0.4, 0.6)$
$\langle p_{T2} \rangle = 0.49$ GeV/c
$p_{T2} \geq 0.6$
$\langle p_{T2} \rangle = 0.78$ GeV/c
$\pi_T(y_1|y_2)$, GeV/c
$\Delta y = y_1 - y_2$

Fig.12